

# Overlap Bias Matching is Necessary for Point Cloud Registration

Pengcheng Shi<sup>1</sup>, Jie Zhang<sup>1</sup>, Haozhe Cheng<sup>1</sup>, Junyang Wang<sup>2</sup>,  
Yiyang Zhou<sup>1</sup>, Chenlin Zhao<sup>3</sup>, Jihua Zhu<sup>1\*</sup>

<sup>1</sup>School of Software Engineering, Xi'an Jiaotong University, Xi'an, China

<sup>2</sup>School of Computer and Information Technology, Beijing Jiaotong University, Beijing, China

<sup>3</sup>State Key Laboratory of Multimodal Artificial Intelligence Systems(MAIS), Institute of Automation, Chinese Academy of Sciences(CASIA), Beijing, China

## Abstract

Point cloud registration is a fundamental problem in many domains. Practically, the overlap between point clouds to be registered may be relatively small. Most unsupervised methods lack effective initial evaluation of overlap, leading to sub-optimal registration accuracy. To address this issue, we propose an unsupervised network Overlap Bias Matching Network (OBMNet) for partial point cloud registration. Specifically, we propose a plug-and-play Overlap Bias Matching Module (OBMM) comprising two integral components, overlap sampling module and bias prediction module. These two components are utilized to capture the distribution of overlapping regions and predict bias coefficients of point cloud common structures, respectively. Then, we integrate OBMM with the neighbor map matching module to robustly identify correspondences by precisely merging matching scores of points within the neighborhood, which addresses the ambiguities in single-point features. OBMNet can maintain efficacy even in pair-wise registration scenarios with low overlap ratios. Experimental results on extensive datasets demonstrate that our approach's performance achieves a significant improvement compared to the state-of-the-art registration approach.

## Introduction

Point cloud registration is a crucial task in the fields of robotics and computer vision. Its primary objective is to align multiple point clouds through appropriate rigid transformations (Agarwal et al. 2011; Schonberger and Frahm 2016). This process finds widespread applications in areas such as 3D map reconstruction, object detection, and autonomous driving (Wong et al. 2017; Deschaud 2018; Zhang and Singh 2014). However, achieving accurate registration becomes challenging due to factors like occlusions, different viewpoints, and inaccurate scanning (Deng, Birdal, and Ilic 2019; Qi et al. 2017b).

In recent years, with the discriminative representation capabilities of deep learning, deep point cloud registration methods have garnered increasing research attention (Tombari, Salti, and Di Stefano 2010; Yang et al. 2017). These methods focus on supervised learning of rigid transformations, requiring a large number of real ground truth transformations as supervised signals for model training (Pais et al. 2020; Fu et al. 2021; Ali et al. 2021; Wang, Li,

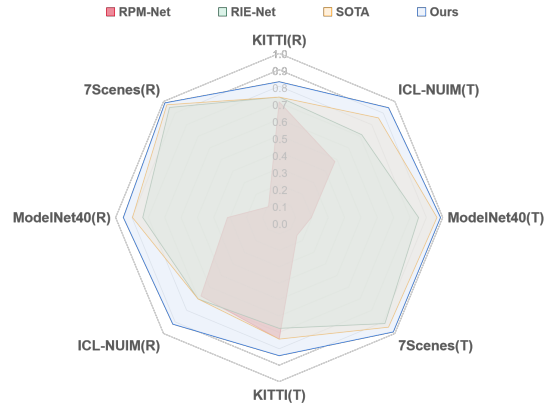


Figure 1: Our method exhibits consistently superior performance across all four datasets through the utilization of min-max normalization.

and Fang 2020). As a result, the training costs escalate, hindering their practical application in real-world scenarios. To address these challenges, various approaches have been proposed. For instance, STORM (Wang et al. 2023) proposed a structure-based overlap matching method for local point cloud registration, detecting overlapping points using structural information and generating precise partial correspondences based on feature similarity. However, the network structure of STORM is complex and requires effective supervision, leading to poor generalization in real point cloud scenes. RIENet (Shen et al. 2022) proposed an unsupervised point cloud registration network with reliable internal evaluation, consisting of a matching refinement module and an internal evaluation module. However, it fails to handle partial-to-partial point cloud registration effectively.

In our paper, we present an Overlap Bias Matching Module (OBMM) suitable for most point cloud registration tasks and propose an unsupervised framework for partial point cloud registration based on this module. Specifically, we use the output of the feature extraction module as the input to OBMM. After passing through a differentiable overlap sampling module, we detect common points in the point cloud using point-wise features to generate partial correspondences. We employ the point cloud structure representing the overlap region along with point-wise features for bias prediction, obtaining matching coefficients for the

\*Corresponding author.

overlapping parts of the two point clouds. These coefficients are used in the weighted SVD for rigid transformation estimation. By fusing global features and locally sampled estimates, we construct a neighbor map matching module to merge the discriminating matching scores of adjacent points to clarify ambiguous single-point features and achieve reliable correspondence recognition. The enriched multi-neighborhood information effectively promotes the construction of the matching graph and provides high-quality correspondences. The experimental results are presented as shown in Figure 1 for demonstration. Our contributions can be summarized as follows:

- We present a plug-and-play Overlap Bias Matching Module (OBMM) consisting of an overlap sampling module and a bias prediction module. This module can effectively analyze the overlapping regions of point clouds in a structured manner and compute bias coefficients.
- We introduce a neighbor map matching module that addresses the ambiguity in single-point matching. An unsupervised point cloud registration network is proposed for partial point clouds by integrating with OBMM.
- Extensive experimental results across a variety of benchmark datasets consistently demonstrate that our method attains state-of-the-art performance in registration.

## Related Work

### Point Cloud Registration

Recently, deep learning has been successfully applied to the point cloud registration which can get the rigid transformation in an end-to-end manner (Fischer et al. 2021; Sarode et al. 2019; Gojcic et al. 2020; Choy, Dong, and Koltun 2020; Bai et al. 2021). There are some supervised methods for point cloud registration through good initial judgment (Lu et al. 2019; Yuan et al. 2020; Sarode et al. 2020; Huang et al. 2021). Following the soft matching map based methods (Wang and Solomon 2019a,b; Mellado, Aiger, and Mitra 2014), RPM-Net (Yew and Lee 2020) uses the Sinkhorn layer to enforce the doubly stochastic constraints on the matching map for reliable correspondences (Li et al. 2020). proposes an iterative distance-aware similarity matrix convolution network with two-stage point elimination technique for point cloud registration. Additionally, there are some end-to-end unsupervised point cloud registration methods (Kadam et al. 2020; Feng et al. 2021; Li, Wang, and Fang 2019; El Banani, Gao, and Johnson 2021; Huang, Mei, and Zhang 2020; Jiang et al. 2021). (Yang et al. 2020; Groueix et al. 2019; Fischler and Bolles 1981) employ cycle consistency across the pairwise point clouds for points matching, which cannot be trained directly on the partial data. RIENet (Shen et al. 2022) introduces an internally assessed unsupervised method for point cloud registration. However, its performance is suboptimal for aligning partial point clouds with low overlap.

### Neighborhood Consensus.

Recently, efforts on neighborhood consensus have been made to establish correspondences between images (Aoki

et al. 2019; Qi et al. 2017a; Li, Pontes, and Lucey 2021; Kadam et al. 2020). Those methods first build a 4D correlation tensor, then employ the 4D CNN on this 4D tensor to achieve the neighborhood consensus (Yang, Li, and Jia 2013; Chen, Hung, and Cheng 1999; Le et al. 2019). Since the 4D tensor are inherently contains neighborhood information, the convolution filters can capture patterns in the pairwise matches of two neighborhoods. However, the operations used in images cannot be directly applied to disordered point clouds. Based on neighborhood consensus, we develop two modules to obtain accurate correspondences and distinguish outliers for robust registration (Phillips, Liu, and Tomasi 2007; Bouaziz, Tagliasacchi, and Pauly 2013; Segal, Haehnel, and Thrun 2009). Since point clouds are disordered and irregular, it cannot directly achieve neighborhood consensus on point clouds with the operations used in images, so we design two modules suitable for point cloud with neighborhood consensus (Rusu et al. 2008; Rusu, Blodow, and Beetz 2009; Tombari, Salti, and Di Stefano 2010). Among them (Yang et al. 2020), with the sparse convolutions and two-stage correspondence relocalisation achieves less memory consumption and more accurate localisation.

## Method

Given a source point cloud  $\mathbf{P} = \{\mathbf{p}_i \in \mathbb{R}^3 \mid i = 1, \dots, N\}$  and a target point cloud  $\mathbf{Q} = \{\mathbf{q}_j \in \mathbb{R}^3 \mid j = 1, \dots, M\}$ . For partial point cloud registration, our proposed method performs feature extraction to generate per-point features  $\Phi_{\mathbf{P}}$  and  $\Phi_{\mathbf{Q}}$  as Figure 2 shows. Global features are constructed as overlapping representations  $\mathbf{T}_{\mathbf{P}}$  and  $\mathbf{T}_{\mathbf{Q}}$  by OBMM, while predicting coefficients  $\alpha$  for the bias distribution of the two frames of overlapping point clouds. By fusing the overlapping representations of point-wise features and global per-point features, we build a matching map  $\mathbf{M}$ . Using the neighbor map matching module, we calculate the relationship coefficients between the target domain and neighboring points, and weight the discriminative matching scores of neighboring points to merge them into the matching graph, thereby obtaining a more reliable corresponding matching map  $\mathbf{M}_r$ . With this, we predict pseudo-target point cloud  $\mathbf{Q}'$ , and through an internal evaluation module, obtain confidence scores  $\mathbf{w}_i$  for each pseudo-matched pair in the target point cloud. Finally, we incorporate the bias coefficient  $\alpha$  as an input to the SVD process for solving the rigid transformation  $\{\mathbf{R}, \mathbf{t}\}$ . This iterative training process continues until a predefined threshold is met.

### Overlap Bias Matching Module

This paper introduces a novel approach utilizing a differential sampling mechanism within an overlap bias matching module for partial point cloud registration. The proposed method comprises an overlap sampling network based on Gumbel-Softmax and a bias prediction sub-network that estimates the current overlap parameters.

**Overlap sampling.** Given the source point cloud  $\mathbf{P}$  and the target point cloud  $\mathbf{Q}$ , in order to enhance the discriminative nature of the learned point-wise features, we employ multiple densely connected EdgeConv layers for feature extrac-

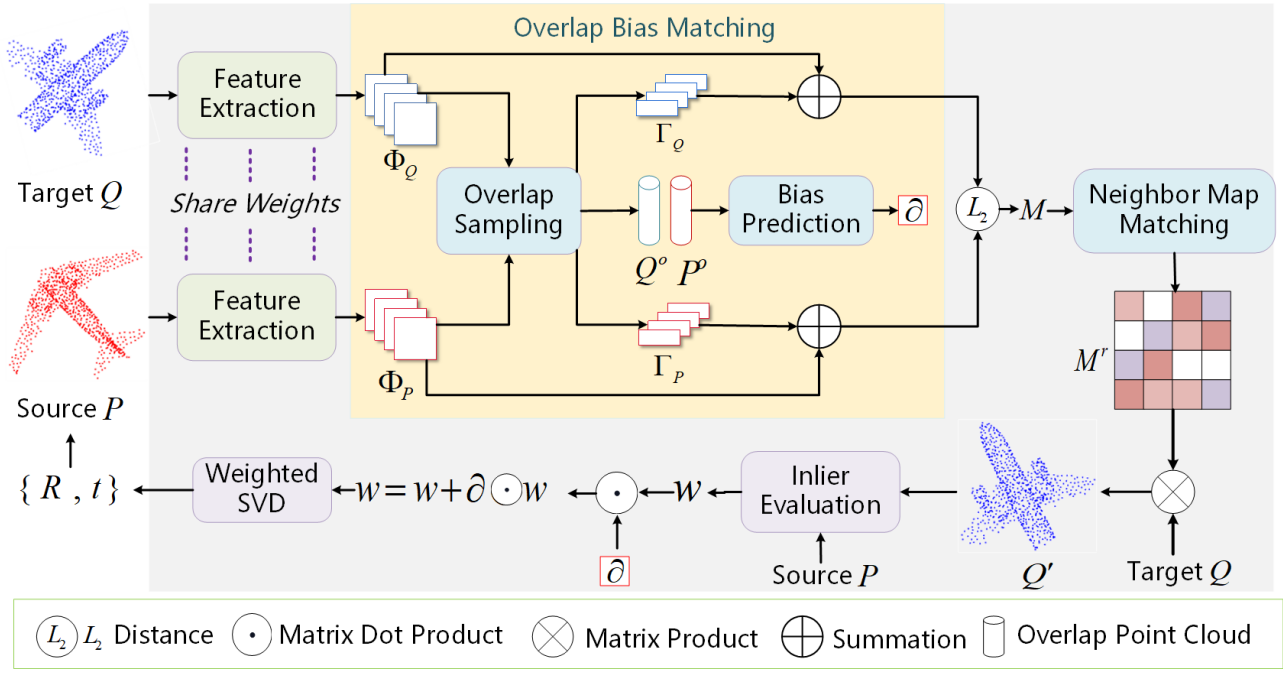


Figure 2: The overall pipeline of OBMNet. Given the input point clouds, It first extracts the point-wise features. Through overlapping sampling, we determine the overlap between the source point cloud  $\mathbf{P}$  and the target point cloud  $\mathbf{Q}$ . Then, we get a bias coefficient  $\alpha$  by bias prediction, which is applied in the subsequent SVD computation. The subsequent neighbor matching module refines the point-wise feature representation, yielding  $M_r$ , which is utilized for generating the pseudo-target point cloud and determining rigid transformations  $\{R, t\}$  in conjunction with  $\alpha$ .

tion, yielding per-point representations  $\Phi_P \in \mathbb{R}^{N \times D}$  and  $\Phi_Q \in \mathbb{R}^{M \times D}$ , where  $N, M$  represents the number of points and  $D$  represents the embedding dimension. These representations are then utilized as inputs to the overlap sampling module, which serves to identify the overlapping regions between point clouds  $\mathbf{P}$  and  $\mathbf{Q}$ . The details of our overlap prediction module are illustrated in Figure 3.

The overlap sampling module relies on a differentiable sampling mechanism. By integrating the feature representations of two frames of point clouds and constructing fully connected layers with adapted channel sizes, we obtain class probabilities  $\pi = \{\pi_1, \dots, \pi_m\}$ . Given the Gumbel noise samples  $g_1 \dots g_m$  drawn from Gumbel(0, 1) distribution and the class probabilities, we can compute a categorical sample  $z$  as follows:

$$z = \text{one\_hot} \left( \arg \max_j [(g_j + \log \pi_j) / \tau] \right), \quad (1)$$

where the parameter  $\tau$  controls the sharpness of the categorical distribution.

We compress the feature representation  $\Phi_P$  of the source point cloud, aligning its dimensions with the input class probabilities, with tensor size tailored to the structure of the original point cloud. Furthermore, in the network architecture, we replace the arg-max operation with a soft-max function approximation, rendering Gumbel-Softmax differentiable. This approach ensures the continuity of the optimization process. Then a distribution indicative of the latent overlapping structure within the input point cloud can be

generated, leading to the visualization of overlapping samples. The sampled points  $Q^o, P^o$  and their corresponding point-wise features  $\Gamma_Q, \Gamma_P \in \mathbb{R}^{K \times D}$  yield the following outcomes:

$$\{Q^o, P^o\} = \text{gumbel\_softmax}(\pi, \tau) \cdot \{Q, P\}, \quad (2)$$

$$\{\Gamma_Q, \Gamma_P\} = \text{Up}(\text{gumbel\_softmax}(\pi, \tau) \cdot \{\Phi_Q, \Phi_P\}), \quad (3)$$

where Up denotes Up-Sampling, and  $K$  represents the number of points sampled from the distribution. It's important to note that each sample is independent. These  $K$  samples represent the overlap between  $\mathbf{P}$  and  $\mathbf{Q}$ .

**Bias prediction.** In previous point cloud registration algorithms, most SVD computations primarily focused on the pseudo-correspondence relationship, while overlooking the bias relationship between two point clouds. To address this, we introduce a secondary neural network that takes two point clouds as inputs and predicts the bias coefficients for the current iteration. These coefficients are then used as weights for the overlapping correspondences during SVD computation. Specifically, we concatenate the two point clouds to form a  $(2N, 4)$  matrix, where the fourth column indicates the origin of each point (from either of the two point clouds) using an extended column containing 0 and 1. This constructed matrix tensor is fed into a series of fully connected layers comprising the point network. To ensure that the predicted  $\alpha$  coefficients are positive, we employ a softplus activation for the final layer as Figure 4 shows.

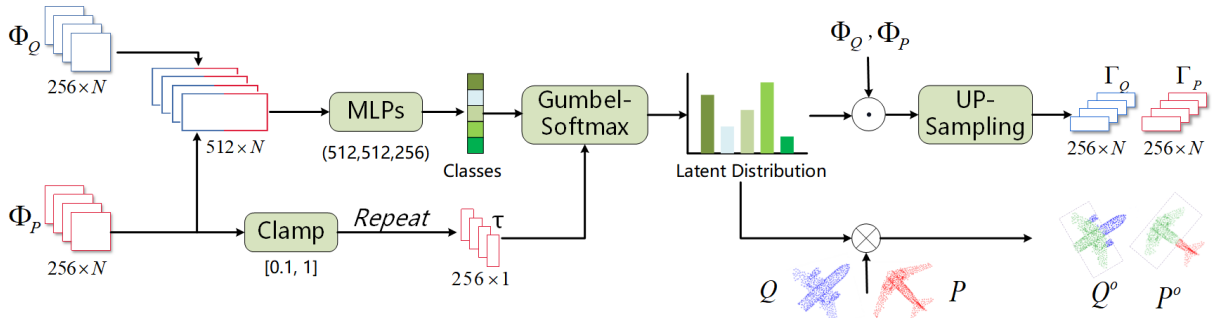


Figure 3: Given the feature inputs  $\Phi_Q$  and  $\Phi_P$ , we first blend the features from two frames, which is achieved by constructing fully connected layers with channel dimensions adapted accordingly. This process yields class probabilities along with a temperature parameter  $\tau$ , which are then employed as inputs for Gumbel-Softmax to derive a distribution describing the latent shared structure within the input point clouds. Finally, we obtain a representation of the overlapping region through sampling.

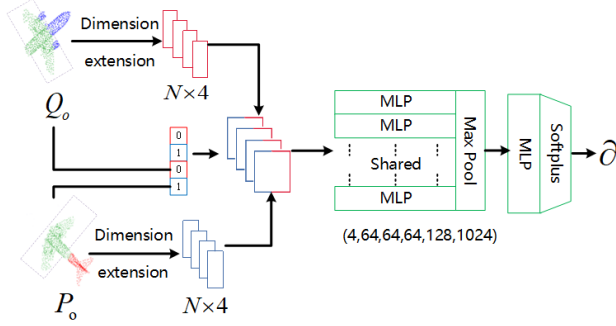


Figure 4: Given the input overlapping point clouds  $Q^o$  and  $P^o$ , we concatenate the feature tensors through dimension extension. This involves augmenting the fourth dimension with columns containing 0 or 1. Afterward, a fully connected layer is utilized to produce the overlap coefficient  $\alpha$  for the two frames of point clouds.

### Neighbor Map Matching Module

Point cloud registration methods based on feature matching often utilize individual point feature distances as scores for constructing matching maps. However, non-corresponding points with similar point features can mislead these methods into making erroneous correspondence estimations. To mitigate this issue, the neighbor map matching module addresses the problem by aggregating discriminative matching scores of neighboring points, thereby enhancing the clarity of ambiguous single-point features and enabling robust correspondence identification. For each point cloud pair  $\mathbf{p}_i$  and  $\mathbf{q}_j$ , we calculate their point-wise matching score with the normalized negative feature distance by calculating the index  $src\_idx$  of  $k$  nearest neighbor points for each point in the input point cloud  $\mathbf{P}$  as below:

$$\mathbf{M}'_{i,j} = \text{softmax}([-M_{i,1}, \dots, -M_{i,M}])_j [src\_idx, :], \quad (4)$$

where  $M_{i,j} = \|\Phi_{\mathbf{p}_i} - \Phi_{\mathbf{q}_j}\|_2$  denotes the euclidean distance between the single-point features of points  $\mathbf{p}_i$  and  $\mathbf{q}_j$ .

Given the matching matrix  $\mathbf{M}'_{i,j}$  as input, we compute

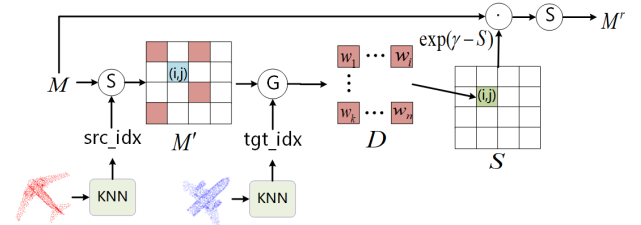


Figure 5: By utilizing the indices of the source point cloud and the target point cloud, combined with a matching map  $M$ . The result  $M^r$  is achieved by weightedly merging the matching scores of neighboring points to refine ambiguous singular point features.

the indices  $tgt\_idx$  of the  $k$  nearest neighbor points for each point in the input point cloud  $\mathbf{Q}$ . Using these index tensors, we gather features and reshape the collected features. We then calculate pairwise distances between these reshaped features, resulting in a weighted distance measure  $\mathbf{D}$ , which is defined as follows:

$$d_{i,j} = \sum_{p_i \in P, j=1}^M \|\text{gather}(\mathbf{M}'_{i,j}, tgt\_idx_i)\|_2^2, \quad (5)$$

$$D_{i,j} = (1/d_{i,j} + \beta) / \left( \sum_{j=1}^M (1/d_{i,j} + \beta) \right),$$

where  $d_{i,j}$  represents pairwise distances between the collected features. The symbol  $\beta$  corresponds to a very small value, typically set to  $e^{-6}$  in practical applications. Based on the estimated point-level matching scores, their neighborhood-level scores can be computed by weighting the corresponding scores of the surrounding points:

$$\mathbf{s}_{i,j} = \frac{D_{i,j}}{K} \sum_{\mathbf{p}_i \in \mathcal{N}_{\mathbf{p}_i}} \sum_{\mathbf{q}_j \in \mathcal{N}_{\mathbf{q}_j}} \mathbf{M}'_{i,j}, \quad (6)$$

where  $\mathcal{N}_{\mathbf{p}_i}$  denotes the  $k$ -nearest neighbor points around the point  $\mathbf{p}_i$ ,  $\mathcal{N}_{\mathbf{q}_j}$  for the same reason. The high neighborhood score means the surrounding points consistently tend to have large matching probabilities and vice versa. Based on the

fact that the real correspondence usually owns the high neighborhood similarity while this similarity for incorrect correspondence is prone to be low, we can effectively exploit this neighborhood score to identify the non-corresponding point pair. Finally, the neighbor matching map can be formulated as:

$$\begin{aligned} \mathbf{M}_{i,j}^r &= \text{softmax}([\mathbf{M}_{i,1}^e, \dots, \mathbf{M}_{i,M}^e])_j, \\ \mathbf{M}_{i,j}^e &= \exp(\gamma - \mathbf{S}_{i,j}) * \mathbf{M}_{i,j}, \end{aligned} \quad (7)$$

where the refined feature distance  $\mathbf{M}_{i,j}^e$  is negatively related to the neighborhood score  $\mathbf{S}_{i,j}$ . and we design an exponential function to control the changing ratio. The hyper-parameter  $\gamma$  controls the influence of the neighborhood consensus. The process is shown in Figure 5.

## Loss Function

In each iteration, we can obtain a set of pseudo correspondences and their corresponding inlier confidence  $\mathbf{w}$ . Then, we employ the weighted SVD on the pseudo correspondences with  $\mathbf{w}$  and  $\alpha$  to estimate the rigid transformation  $\{\mathbf{R}, \mathbf{t}\}$ . Under the unsupervised setting, we construct the following unsupervised loss functions for model optimization.

**Global alignment loss.** We first exploit the alignment error based loss function to train our model. To handle the partially-overlapping problem well, we integrate the Huber function, a robust loss function insensitive to the outliers. The Huber function based overall alignment loss can be formulated as:

$$\begin{aligned} \mathcal{L}_g &= \sum_{\mathbf{p}_i' \in \mathbf{P}'} \vartheta \left( \min_{\mathbf{q}_i \in \mathbf{Q}} \|\mathbf{p}_i' - \mathbf{q}_i\|_2^2 \right) \\ &+ \sum_{\mathbf{q}_i \in \mathbf{Q}} \vartheta \left( \min_{\mathbf{p}_i' \in \mathbf{P}'} \|\mathbf{q}_i - \mathbf{p}_i'\|_2^2 \right), \end{aligned} \quad (8)$$

where  $\mathbf{P}'$  denotes the transformed source point cloud with the estimated transformation and  $\vartheta$  is the huber function.

**Neighborhood agreement loss.** To prevent the model from becoming trapped in local optima, we introduce the robust KNN-based neighborhood consensus loss along with the spatial consistency loss, aimed at further mitigating the impact of outliers. By selecting the  $k$  pairs of points with the highest weights determined through overlap prediction, we acquire overlapping point clouds:  $\mathbf{X} \in \mathbb{R}^{k \times 3}$  and  $\mathbf{Y} \in \mathbb{R}^{k \times 3}$ . This enables us to formulate the neighborhood agreement loss using the transformation  $\{\mathbf{R}, \mathbf{t}\}$ :

$$\mathcal{L}_n = \sum_{\mathbf{x}_i \in \mathbf{X}, \mathbf{y}_i \in \mathbf{Y}} \sum_{\mathbf{p}_j \in \mathcal{N}_{\mathbf{x}_i}, \mathbf{q}_j \in \mathcal{N}_{\mathbf{y}_i}} \|\mathbf{R}\mathbf{p}_j + \mathbf{t} - \mathbf{q}_j\|_2. \quad (9)$$

**Spatial consistency loss.** In order to further eliminate the spatial gap between the pseudo target correspondence and the real target correspondence for each selected  $\mathbf{x}_i \in \mathbf{X}$ , we exploit the cross-entropy based spatial consistency loss to

sharpen their matching distributions as below:

$$\mathcal{L}_s = -\frac{1}{|\mathbf{X}|} \sum_{\mathbf{x}_i \in \mathbf{X}} \sum_{j=1}^M \mathbb{I} \left\{ j = \arg \max_{j'} \mathbf{M}_{i,j'}^r \right\} \log \mathbf{M}_{i,j}^r, \quad (10)$$

where  $\mathbb{I}\{\cdot\}$  denotes the indicator function and we use the target point  $\mathbf{q}_j$  with the largest matching probability to estimate the real target correspondence. By improving the matching probability of the “real” target correspondence ( $\mathbf{M}_{i,j}^r \rightarrow 1$ ), the resulting pseudo target correspondence tends to further spatially approach to the “real” target correspondence  $\mathbf{q}_j$  well. Finally, we utilize a comprehensive loss function as below to optimize our model:

$$\mathcal{L} = \mathcal{L}_g + \mathcal{L}_n + \mathcal{L}_s. \quad (11)$$

## Experiments

### Experimental Settings

**Datasets.** We evaluate our method on ModelNet40 (Wu et al. 2015), 7Scenes (Shotton et al. 2013), ICL-NUIM (Choi, Zhou, and Koltun 2015) and KITTI odometry datasets (Geiger, Lenz, and Urtasun 2012). The ModelNet40 consists of 12,311 meshed CAD models from 40 categories. We use 9,843 models for training and 2,468 models for testing. 7Scenes is a widely used benchmark registration dataset of indoor environment with 7 scenes including Chess, Fires, Heads, Office, Pumpkin, RedKitchen and Stairs. The dataset is divided into 296 samples for training and 57 for testing. For another synthetic indoor scene ICL-NUIM, we first augment the dataset, then split the dataset into 1,278 samples for training and 200 samples for testing. And the KITTI odometry dataset consists of 11 sequences with ground truth pose, we use Sequence 00-05 for training, 06-07 for validation, and 08-10 for testing. We form the pairwise point clouds with the current frame and the 10th frame after it.

**Compared methods and evaluation metrics.** We compare with traditional methods including ICP (Besl and McKay 1992), FGR (Zhou, Park, and Koltun 2016). Besides, we compare with deep methods, including supervised DCP (Wang and Solomon 2019a), IDAM (Li et al. 2020), RPM-Net (Yew and Lee 2020) and STORM (Wang et al. 2023), and unsupervised RIENet (Shen et al. 2022). We evaluate the registration by the mean absolute errors (MAE) of  $\mathbf{R}$  and  $\mathbf{t}$ , which are anisotropic, and the mean isotropic errors (MIE) of  $\mathbf{R}$  and  $\mathbf{t}$  used in RIENet.

**Implementation details.** Our model is implemented in Pytorch. We optimize the parameters with the ADAM optimizer. The initial learning rate is 0.001. For ModelNet40 and KITTI, we train the network for 50 epochs and multiply the learning rate by 0.7 at epoch 25. For indoor scenes, we multiply the learning rate by 0.7 at epochs 25, 50, 75 and train the network for 100 epochs.

### Comparison Evaluation

**Analysis.** We compared the registration performance of different methods on the ModelNet40 dataset under scenarios

Model	Same				Unseen				Noise			
	MAE(R)	MAE(t)	MIE(R)	MIE(t)	MAE(R)	MAE(t)	MIE(R)	MIE(t)	MAE(R)	MAE(t)	MIE(R)	MIE(t)
ICP	3.4339	0.0114	6.7706	0.0227	3.6099	0.0116	7.0556	0.0228	4.6441	0.0167	9.2194	0.0333
FGR	0.5972	0.0021	1.1563	0.0041	0.4579	0.0016	0.8442	0.0032	1.0676	0.0036	2.0038	0.0072
DCP	1.3405	0.0075	3.4980	0.0070	1.7736	0.0093	3.8657	0.0090	2.7653	0.0137	5.7763	0.0279
IDAM	0.4243	0.0020	0.8170	0.0040	0.4809	0.0028	0.9157	0.0055	2.3076	0.0124	4.5332	0.0246
RPM-Net	0.0051	0.00005	0.0201	0.00006	0.0064	0.00014	0.0207	0.00014	0.0075	0.0000	0.0221	0.0001
STORM	0.0037	0.00002	0.0341	0.00005	0.0052	0.00004	0.0415	0.00008	0.0067	0.00016	0.0248	<b>0.00014</b>
RIENet	0.0033	0.00004	0.0210	0.00005	0.0059	0.00004	0.0228	0.00011	0.0069	<b>0.00014</b>	0.0230	0.00016
Ours	<b>0.0013</b>	<b>0.00001</b>	<b>0.0190</b>	<b>0.00003</b>	<b>0.0016</b>	<b>0.00001</b>	<b>0.0192</b>	<b>0.00003</b>	<b>0.0048</b>	<b>0.00014</b>	<b>0.0221</b>	0.00015

Table 1: The registration results of different methods on ModelNet40.

Model	ICL-NUIM				7Scenes				KITTI			
	MAE(R)	MAE(t)	MIE(R)	MIE(t)	MAE(R)	MAE(t)	MIE(R)	MIE(t)	MAE(R)	MAE(t)	MIE(R)	MIE(t)
ICP	2.4022	0.0699	4.4832	0.1410	6.0091	0.0130	13.0484	0.0260	4.7433	0.9174	11.9982	2.5732
FGR	2.2477	0.0808	4.1850	0.1573	0.0919	0.0004	0.1705	0.0008	1.6777	0.0352	4.0467	0.0762
DCP	5.7619	0.1762	8.8611	0.2561	3.6518	0.0243	10.0324	0.0557	4.3207	0.0402	8.1679	0.0817
IDAM	4.4153	0.1385	8.6178	0.2756	5.6727	0.0303	11.5949	0.0629	1.6348	0.0230	3.8151	0.0491
RPM-Net	0.3267	0.0125	0.6277	0.0246	0.3885	0.0021	0.7649	0.0042	0.9164	0.0146	2.1291	0.0303
STORM	0.0311	0.0017	0.1068	0.0057	0.0304	0.0002	0.0354	0.0001	0.6624	0.0147	2.0765	0.0512
RIENet	0.0492	0.0023	0.0897	0.0049	0.0121	0.0001	0.0299	0.0001	0.8251	0.0183	1.8754	0.0414
Ours	<b>0.0210</b>	<b>0.0013</b>	<b>0.0664</b>	<b>0.0038</b>	<b>0.0053</b>	<b>0.000034</b>	<b>0.02304</b>	<b>0.000068</b>	<b>0.5237</b>	<b>0.0103</b>	<b>1.5884</b>	<b>0.0393</b>

Table 2: The registration results of different methods on the indoor scenes and outdoor dataset.

Model	ModelNet40				KITTI			
	MAE(R)	MAE(t)	MIE(R)	MIE(t)	MAE(R)	MAE(t)	MIE(R)	MIE(t)
ICP	11.67	0.16	23.04	0.33	15.37	12.65	39.67	30.10
FGR	4.74	0.062	9.53	0.128	17.23	1.3348	38.85	3.004
DCP	3.76	0.059	7.01	0.062	10.24	0.388	22.09	0.864
IDAM	7.02	0.110	14.86	0.233	18.09	0.8958	34.85	1.742
RPM-Net	0.97	0.0064	3.12	0.0071	3.94	0.0976	7.26	0.305
STORM	0.134	0.00058	1.43	0.0017	1.27	0.0237	3.25	0.0867
RIENet	0.174	0.00062	0.88	0.0043	3.19	0.0664	5.15	0.177
Ours	<b>0.057</b>	<b>0.00026</b>	<b>0.62</b>	<b>0.0007</b>	<b>1.05</b>	<b>0.0195</b>	<b>2.85</b>	<b>0.0574</b>

Table 3: The registration results of different methods on ModelNet40 and KITTI with overlap rate of 0.58.

of “Same categories”, “Unseen categories” and “Noise categories”, as shown in Table 1. Each source point cloud, denoted as P, in the training set, is transformed into Q using randomly generated transformation matrices. It can be observed that as an unsupervised learning approach, our method achieves the smallest errors among both traditional and deep learning methods.

We validated our approach on various real-world datasets, including ICL-NUIM and 7Scenes for indoor scenes, as well as KITTI for outdoor scenes. Following the data processing in RIENet, our model shows promising performance in both indoor and outdoor scenarios, as shown in Table 2. While

Model	ModelNet40			
	MAE(R)	MAE(t)	MIE(R)	MIE(t)
OBMM+FGR	0.2714	0.0010	0.8236	0.0028
OBMM+DCP	0.8842	0.0050	2.1410	0.0049
OBMM+IDAM	0.0954	0.0008	0.1956	0.0009
OBMM+RPM-Net	0.0050	0.00004	0.0221	0.00006

Table 4: The registration results of different methods combined with OBMM on ModelNet40.

the STORM method exhibits similarities with our approach in certain metrics, our method boasts nearly 1/5 of its run-time. The visual outcomes across four distinct datasets are depicted in Figure 6.

**Partial object registration.** To validate the effectiveness of our method in partial-to-partial registration, we conducted experiments on the sparsely overlapped ModelNet40 and KITTI datasets. By employing a truncation approach, we generated point clouds with an approximate overlap rate of 0.58, where the point cloud overlap rate is defined as the ratio of point pairs in similar spatial positions to the total number of points. The experimental results, as presented in Table 3, demonstrate our method’s capability to accurately detect point cloud overlap and generate partial correspondences. In comparison to other approaches, our method exhibits a notably pronounced advantage.



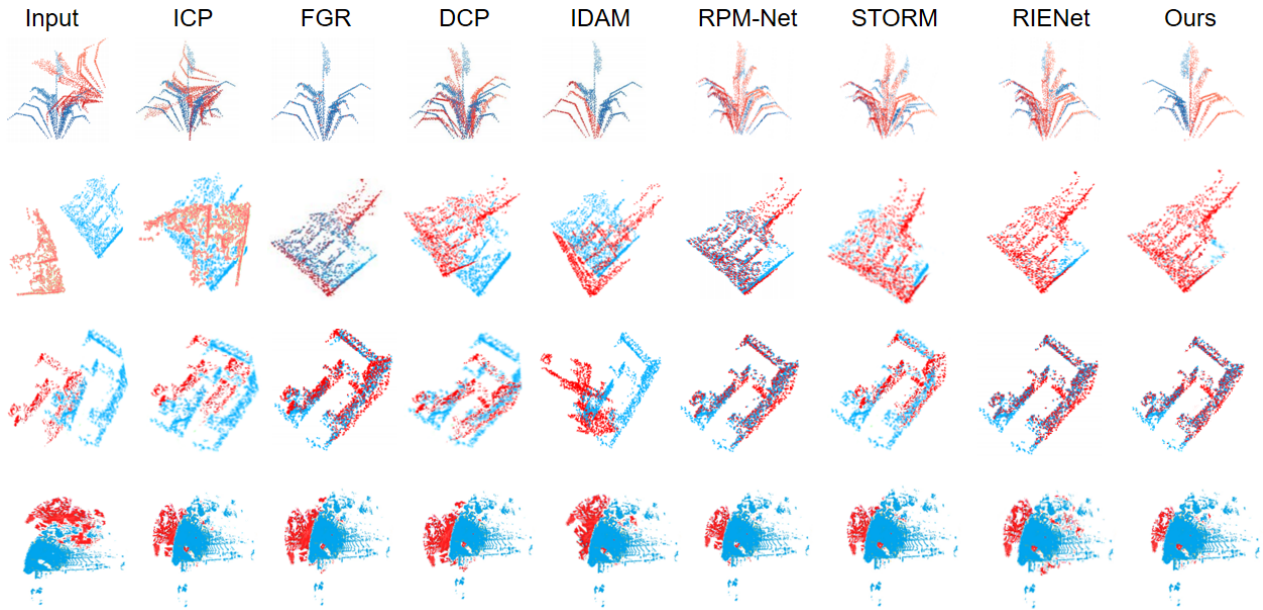


Figure 6: Visualization of registration results on the ModelNet40, 7Scenes, ICL-NUIM and KITTI datasets.

NMM	OS	BP	MAE(R)	MAE(t)	MIE(R)	MIE(t)
	✓	✓	0.0124	0.000035	0.098	0.000086
✓			0.0058	0.000037	0.022	0.000103
✓	✓		0.0043	0.000028	0.022	0.000052
✓	✓	✓	<b>0.0016</b>	<b>0.000014</b>	<b>0.019</b>	<b>0.000031</b>

Table 5: The results of different combination of key components on ModelNet40.

**Transferrability of OBMM.** OBMM demonstrates impressive transferability, effectively improving the precision of various deep methods for partial-to-partial registration. We integrated OBMM into FGR, DCP, IDAM, and RPM-Net as an overlap feature extractor for point clouds. By predicting overlap biases, we introduced bias coefficients into the subsequent network to aid matrix transformation. The results in Table 4 clearly illustrate the substantial enhancement in registration accuracy achieved through OBMM integration. Remarkably, this improvement comes without significant additional runtime overhead.

### Ablation Study

**The effectiveness of key components.** We conducted an ablation study on the three key components of this model: Overlapping Sampling (OS), Bias Prediction (BP), and Neighbor Map Matching (NMM) modules. In the baseline configuration, we concatenated the point-wise features of the encoder and used them as input for the MLP, thereby replacing the OS module and eliminating the NMM module. The baseline model was trained using our unsupervised loss function. By incrementally adding these components, we obtained results for different categories on ModelNet40

Loss	MAE(R)	MAE(t)	MIE(R)	MIE(t)
$\mathcal{L}_g$	2.0456	0.9888	74.2689	5.6725
$\mathcal{L}_g + \mathcal{L}_s$	4.8653	0.2195	14.8652	1.1569
$\mathcal{L}_g + \mathcal{L}_s + \mathcal{L}_n$	<b>0.5237</b>	<b>0.0103</b>	<b>1.5884</b>	<b>0.0393</b>

Table 6: The results of different combination of loss functions on KITTI.

dataset. The outcomes are presented in Table 5. Notably, the early OS module exhibits significant improvements over the baseline. Furthermore, the neighbor map matching module contributes to achieving more precise partial data registration results.

**Loss functions.** In our experiments, we train our model with the combination of the global alignment loss  $\mathcal{L}_g$ , the neighborhood agreement loss  $\mathcal{L}_n$ , and the spatial consistency loss  $\mathcal{L}_s$ . In Table 6, we train our model using the different loss functions and present the results on KITTI. One can see that with the neighborhood consensus loss and spatial consistency loss based on the selected module, we can obtain high registration precision.

### Conclusion

In this paper, we propose a plug-and-play Overlap Bias Matching Module (OBMM) and then integrate it with the neighbor map matching module to construct an unsupervised network for partial point cloud registration. The OBMM comprises two components: a differentiable overlap sampling module and a bias prediction module. The proposed OBMM has good generalization and can be easily integrated into most registration networks. By integrating OBMM and the neighbor map matching module, we

have devised an unsupervised point cloud registration network. This network can maintain efficacy even in pair-wise registration scenarios with low overlap ratios. Experimental results on extensive datasets demonstrate that our method achieves state-of-the-art registration performance.

## References

- Agarwal, S.; Furukawa, Y.; Snavely, N.; Simon, I.; Curless, B.; Seitz, S. M.; and Szeliski, R. 2011. Building rome in a day. *Communications of the ACM*, 54(10): 105–112.
- Ali, S. A.; Kahraman, K.; Reis, G.; and Stricker, D. 2021. RPSRNet: End-to-End Trainable Rigid Point Set Registration Network using Barnes-Hut 2D-Tree Representation. In *CVPR*.
- Aoki, Y.; Goforth, H.; Srivatsan, R. A.; and Lucey, S. 2019. PointNetLK: Robust & efficient point cloud registration using pointnet. In *CVPR*.
- Bai, X.; Luo, Z.; Zhou, L.; Chen, H.; Li, L.; Hu, Z.; Fu, H.; and Tai, C.-L. 2021. PointDSC: Robust Point Cloud Registration using Deep Spatial Consistency. In *CVPR*.
- Besl, P. J.; and McKay, N. D. 1992. Method for registration of 3-D shapes. In *SPIE*.
- Bouaziz, S.; Tagliasacchi, A.; and Pauly, M. 2013. Sparse iterative closest point. In *Computer graphics forum*, volume 32, 113–123.
- Chen, C.-S.; Hung, Y.-P.; and Cheng, J.-B. 1999. RANSAC-based DARCES: A new approach to fast automatic registration of partially overlapping range images. *IEEE Transactions on Pattern Analysis and Machine Intelligence*, 21(11): 1229–1234.
- Choi, S.; Zhou, Q.-Y.; and Koltun, V. 2015. Robust reconstruction of indoor scenes. In *CVPR*.
- Choy, C.; Dong, W.; and Koltun, V. 2020. Deep Global Registration. In *CVPR*.
- Deng, H.; Birdal, T.; and Ilic, S. 2019. 3D local features for direct pairwise registration. In *CVPR*.
- Deschaud, J.-E. 2018. IMLS-SLAM: scan-to-model matching based on 3D data. In *ICRA*.
- El Banani, M.; Gao, L.; and Johnson, J. 2021. Unsuperviseddr: Unsupervised point cloud registration via differentiable rendering. In *CVPR*.
- Feng, W.; Zhang, J.; Cai, H.; Xu, H.; Hou, J.; and Bao, H. 2021. Recurrent Multi-view Alignment Network for Unsupervised Surface Registration. In *CVPR*.
- Fischer, K.; Simon, M.; Olsner, F.; Milz, S.; Gross, H.-M.; and Mader, P. 2021. Stickypillars: Robust and efficient feature matching on point clouds using graph neural networks. In *CVPR*.
- Fischler, M. A.; and Bolles, R. C. 1981. Random sample consensus: a paradigm for model fitting with applications to image analysis and automated cartography. *Communications of the ACM*, 24(6): 381–395.
- Fu, K.; Liu, S.; Luo, X.; and Wang, M. 2021. Robust Point Cloud Registration Framework Based on Deep Graph Matching. In *CVPR*.
- Geiger, A.; Lenz, P.; and Urtasun, R. 2012. Are we ready for autonomous driving? the kitti vision benchmark suite. In *CVPR*.
- Gojcic, Z.; Zhou, C.; Wegner, J. D.; Guibas, L. J.; and Birdal, T. 2020. Learning multiview 3D point cloud registration. In *CVPR*.
- Groueix, T.; Fisher, M.; Kim, V. G.; Russell, B. C.; and Aubry, M. 2019. Unsupervised cycle-consistent deformation for shape matching. In *Computer Graphics Forum*, volume 38, 123–133.
- Huang, S.; Gojcic, Z.; Usvyatsov, M.; Wieser, A.; and Schindler, K. 2021. PREDATOR: Registration of 3D Point Clouds with Low Overlap. In *CVPR*.
- Huang, X.; Mei, G.; and Zhang, J. 2020. Feature-metric Registration: A Fast Semi-supervised Approach for Robust Point Cloud Registration without Correspondences. In *CVPR*.
- Jiang, H.; Shen, Y.; Li, J.; Qian, J.; Xie, J.; and Yang, J. 2021. Sampling Network Guided Cross-Entropy Method for Unsupervised Point Cloud Registration. In *ICCV*.
- Kadam, P.; Zhang, M.; Liu, S.; and Kuo, C.-C. J. 2020. Unsupervised Point Cloud Registration via Salient Points Analysis (SPA). In *VCIP*.
- Le, H. M.; Do, T.-T.; Hoang, T.; and Cheung, N.-M. 2019. Sdrsac: Semidefinite-based randomized approach for robust point cloud registration without correspondences. In *CVPR*.
- Li, J.; Zhang, C.; Xu, Z.; Zhou, H.; and Zhang, C. 2020. Iterative distance-aware similarity matrix convolution with mutual-supervised point elimination for efficient point cloud registration. In *Computer Vision—ECCV 2020: 16th European Conference, Glasgow, UK, August 23–28, 2020, Proceedings, Part XXIV 16*, 378–394. Springer.
- Li, X.; Pontes, J. K.; and Lucey, S. 2021. PointNetLK Revisited. In *CVPR*.
- Li, X.; Wang, L.; and Fang, Y. 2019. Pc-net: Unsupervised point correspondence learning with neural networks. In *3DV*.
- Lu, W.; Wan, G.; Zhou, Y.; Fu, X.; Yuan, P.; and Song, S. 2019. DeepVCP: An End-to-End Deep Neural Network for Point Cloud Registration. In *ICCV*.
- Mellado, N.; Aiger, D.; and Mitra, N. J. 2014. Super 4pcs fast global pointcloud registration via smart indexing. In *Computer graphics forum*, volume 33, 205–215.
- Pais, G. D.; Ramalingam, S.; Govindu, V. M.; Nascimento, J. C.; Chellappa, R.; and Miraldo, P. 2020. 3DRegNet: A deep neural network for 3D point registration. In *CVPR*.
- Phillips, J. M.; Liu, R.; and Tomasi, C. 2007. Outlier robust ICP for minimizing fractional RMSD. In *3DIM*.
- Qi, C. R.; Su, H.; Mo, K.; and Guibas, L. J. 2017a. PointNet: Deep learning on point sets for 3D classification and segmentation. In *CVPR*.
- Qi, C. R.; Yi, L.; Su, H.; and Guibas, L. J. 2017b. PointNet++: Deep hierarchical feature learning on point sets in a metric space. In *NIPS*.
- Rusu, R. B.; Blodow, N.; and Beetz, M. 2009. Fast point feature histograms (FPFH) for 3D registration. In *ICRA*.



- Rusu, R. B.; Blodow, N.; Marton, Z. C.; and Beetz, M. 2008. Aligning point cloud views using persistent feature histograms. In *IROS*.
- Sarode, V.; Dhagat, A.; Srivatsan, R. A.; Zevallos, N.; Lucey, S.; and Choset, H. 2020. MaskNet: A Fully-Convolutional Network to Estimate Inlier Points. *arXiv preprint arXiv:2010.09185*.
- Sarode, V.; Li, X.; Goforth, H.; Aoki, Y.; Srivatsan, R. A.; Lucey, S.; and Choset, H. 2019. PCRNet: Point cloud registration network using PointNet encoding. *arXiv preprint arXiv:1908.07906*.
- Schonberger, J. L.; and Frahm, J.-M. 2016. Structure-from-motion revisited. In *CVPR*.
- Segal, A.; Haehnel, D.; and Thrun, S. 2009. Generalized-icp. In *RSS*.
- Shen, Y.; Hui, L.; Jiang, H.; Xie, J.; and Yang, J. 2022. Reliable Inlier Evaluation for Unsupervised Point Cloud Registration. *arXiv e-prints*.
- Shotton, J.; Glocker, B.; Zach, C.; Izadi, S.; Criminisi, A.; and Fitzgibbon, A. 2013. Scene coordinate regression forests for camera relocalization in RGB-D images. In *CVPR*.
- Tombari, F.; Salti, S.; and Di Stefano, L. 2010. Unique shape context for 3D data description. In *ACM workshop*.
- Wang, L.; Li, X.; and Fang, Y. 2020. Unsupervised Learning of 3D Point Set Registration. *arXiv preprint arXiv:2006.06200*.
- Wang, Y.; and Solomon, J. M. 2019a. Deep closest point: Learning representations for point cloud registration. In *Proceedings of the IEEE/CVF international conference on computer vision*, 3523–3532.
- Wang, Y.; and Solomon, J. M. 2019b. PRNet: Self-supervised learning for partial-to-partial registration. In *NIPS*.
- Wang, Y.; Yan, C.; Feng, Y.; Du, S.; Dai, Q.; and Gao, Y. 2023. STORM: Structure-Based Overlap Matching for Partial Point Cloud Registration. *IEEE Transactions on Pattern Analysis and Machine Intelligence*, 45(1): 1135–1149.
- Wong, J. M.; Kee, V.; Le, T.; Wagner, S.; Mariottini, G.-L.; Schneider, A.; Hamilton, L.; Chipalkatty, R.; Hebert, M.; Johnson, D. M.; et al. 2017. SegICP: Integrated deep semantic segmentation and pose estimation. In *IROS*.
- Wu, Z.; Song, S.; Khosla, A.; Yu, F.; Zhang, L.; Tang, X.; and Xiao, J. 2015. 3D ShapeNets: A Deep Representation for Volumetric Shapes. In *CVPR*.
- Yang, J.; Li, H.; and Jia, Y. 2013. Go-ICP: Solving 3D Registration Efficiently and Globally Optimally. In *ICCV*.
- Yang, L.; Liu, W.; Cui, Z.; Chen, N.; and Wang, W. 2020. Mapping in a cycle: Sinkhorn regularized unsupervised learning for point cloud shapes. In *ECCV*.
- Yang, Y.; Feng, C.; Shen, Y.; and Tian, D. 2017. Foldingnet: Interpretable unsupervised learning on 3d point clouds. *arXiv preprint arXiv:1712.07262*.
- Yew, Z. J.; and Lee, G. H. 2020. RPM-Net: Robust Point Matching using Learned Features. In *CVPR*.
- Yuan, W.; Eckart, B.; Kim, K.; Jampani, V.; Fox, D.; and Kautz, J. 2020. Deepgmr: Learning latent gaussian mixture models for registration. In *ECCV*.
- Zhang, J.; and Singh, S. 2014. LOAM: Lidar Odometry and Mapping in Real-time. In *RSS*.
- Zhou, Q.-Y.; Park, J.; and Koltun, V. 2016. Fast global registration. In *ECCV*.